



PAPER

Ultrafast spectroscopy of voltage reconfigurable graphene saturable absorbers in the visible and near infrared

RECEIVED
8 January 2019ACCEPTED FOR PUBLICATION
1 April 2019PUBLISHED
23 April 2019I Baylam¹, M N Cizmeciyan¹, N Kakenov², C Kocabas^{2,3} and A Sennaroglu^{1,4,5}¹ Koç University Surface Science and Technology Center (KUYTAM), Rumelifeneri, Istanbul 34450, Turkey² Department of Physics, Bilkent University, Ankara 06800, Turkey³ School of Materials and National Graphene Institute, the University of Manchester, Oxford Rd, Manchester, M13 9PL, United Kingdom⁴ Departments of Physics and Electrical-Electronics Engineering, Laser Research Laboratory, Koç University, Istanbul 34450, Turkey⁵ Author to whom any correspondence should be addressed.E-mail: asenнар@ku.edu.tr**Keywords:** graphene saturable absorbers, ultrafast spectroscopy, 2D materials**Abstract**

We describe a detailed experimental investigation of the ultrafast nonlinear response of a voltage-controlled graphene-gold saturable absorber (VCG-gold-SA) by employing femtosecond pump probe spectroscopy. Visible and near-infrared continuum probe pulses covering the spectral range from 500 nm to 1600 nm were used. In the experiments, the saturation fluence, modulation depth, ultrafast relaxation times, and the saturable absorption bandwidth of the VCG-gold-SA were measured as a function of the applied bias. We observed both saturable absorption and multi-photon absorption regimes as the applied bias voltage was varied between 0 and 2 V. Measurements indicate that under bias voltages in the range of 0–2 V, it should be possible to adjust the insertion loss of the VCG-gold-SA and at the same time, maintain a sufficient amount of modulation depth as well as an attainable level of saturation fluence over an ultrabroad spectral bandwidth. In particular, at the bias voltage of 1 V, the VCG-gold-SA exhibited fast saturable absorber behavior with adjustable insertion loss from 630 nm to 1100 nm. These results clearly demonstrate that the VCG-gold-SA can operate as a versatile mode locker for femtosecond pulse generation from lasers operating in the visible and near-infrared wavelengths.

1. Introduction

An important member of the 2D layered materials, graphene possesses unique optical properties that have been explored in many applications [1–12]. In particular, the ultrafast nonlinear response of undoped and doped graphene has been investigated with various combinations of pump-probe wavelengths ranging from the ultraviolet to the terahertz region [13–23]. Recent studies have also demonstrated that the optical response of graphene can be modified by varying the position of the Fermi level with external bias in capacitor structures. Use of capacitor architectures offers the advantage of continuous and reversible adjustment of absorption, which cannot be achieved by chemical doping, where the shift in the Fermi level and the resulting change in the absorption are fixed. Such voltage reconfigurable graphene devices with adjustable (tunable), bias-dependent optical response have numerous potential applications as have been demonstrated in recent studies involving the

stabilization of optical frequency combs [24], optical modulation from visible to microwave wavelengths [25–33], electrically-switchable radar absorption [34], modulation in flexible electronics [35], gate-tunable control of nonlinear phase shifts [36], gate-tunable third harmonic generation [37], and four-wave mixing [38].

Another recently emerging and exciting application of voltage reconfigurable graphene is in femtosecond pulse generation from lasers. It is well known that monolayer or few-layer graphene can be used as a fast saturable absorber over an ultrabroad spectral range (750 nm–2800 nm) to initiate mode-locked operation of lasers and to generate ultrashort optical pulses [39–47]. Voltage reconfigurable graphene offers an additional important advantage because its insertion loss (2.3% per transit in monolayer graphene) can be continuously adjusted with applied bias, while maintaining fast saturable absorber action, so that it can be used inside lasers with relatively low optical gain. Furthermore, by using supercapacitor structures

with a high dielectric constant electrolyte between the graphene electrodes, the Fermi level and hence, the loss level can be adjusted with low bias voltages in the 0–2 V range [48–51]. This is another important advantage of the graphene supercapacitor structures since the operating voltage range becomes considerably lower than that of solid-state graphene capacitors. Recent investigations have shown that an optimum architecture for a voltage-reconfigurable graphene supercapacitor saturable absorber consists of a graphene electrode, a notched gold electrode, and a high dielectric-constant electrolyte in between [48, 49]. In the remainder of this paper, we will refer to this structure as the voltage-controlled graphene-gold saturable absorber (VCG-gold-SA). In general, the nonlinear optical response of these devices will vary with the applied bias and the resulting shift in the Fermi level. Hence, it is important to experimentally determine the spectral region over which the device maintains its fast saturable absorber function and how the saturation characteristics such as saturation fluence, modulation depth, and relaxation times vary at different levels of bias.

In this paper, we provide a detailed experimental investigation of the ultrafast nonlinear response of a voltage-controlled graphene-gold saturable absorber (VCG-gold-SA) by employing femtosecond pump-probe spectroscopy. Visible and near-infrared continuum probe pulses covering the spectral range from 500 nm to 1600 nm were used. In the experiments, the saturation fluence, modulation depth, ultrafast relaxation times, and the saturable absorption bandwidth of the VCG-gold-SA were measured as a function of the applied bias. We observed both saturable absorption and multi-photon absorption regimes as the applied bias voltage was varied between 0 and 2 V. In particular, at a given photon energy, the measurements show that there is a maximum applied bias beyond which one-photon interband transition of the carriers completely vanishes due to Pauli blocking and the VCG-gold-SA no longer operates as a fast saturable absorber. Measurements indicated that with increasing bias voltage, the saturable absorption bandwidth decreased but remained wide enough to support femtosecond pulse generation in the visible and near-infrared wavelengths. For example, at the bias voltage of 1 V, the VCG-gold-SA could be operated as a fast saturable absorber with adjustable insertion loss over the wavelength range of 630–1100 nm. Furthermore, the voltage-dependent saturation fluence and modulation depth measurements were in agreement with the previously reported theoretical predictions [52, 53].

2. Methods

Figure 1(a) shows a sketch of the voltage-controlled graphene-gold saturable absorber (VCG-gold-SA) used in the femtosecond pump-probe spectroscopy measurements. The graphene electrode of the supercapacitor was synthesized via chemical vapor

deposition (CVD) and the monolayer graphene was transferred onto a quartz substrate. Detailed characterization measurements of a similar monolayer graphene were carried out in previous studies by using atomic force microscopy, Raman spectroscopy, and scanning electron microscopy [35]. The second electrode consisted of a quartz plate coated with gold using thermal evaporation. Gold has been our primary choice as the conducting electrode because of its chemical inertness and wide availability. A circular notch with a 5 mm diameter was patterned on the gold electrode to allow the transit of the laser beam through the structure. An ionic liquid (Diethymethyl (2-methoxyethyl) ammonium bis (trifluoro-methylsulfonyl) imide [DEME][TFSI]) with a relative dielectric constant of $\epsilon_r = 14$ was used to fill the 100 μm -thick space between the graphene and the gold electrodes. Our measurements showed that under a given bias, the measured change in the optical transmission of the sample was fairly uniform across the notch, suggesting a uniform shift in the Fermi level over the notch [48]. However, the presence of the gold electrode caused an unintentional Fermi level shift of 0.5 eV due to the work function mismatch between the graphene and the gold electrodes. Additional details about the fabrication and characterization of a similar VCG-gold-SA can be found in [31, 49].

Optical transitions from the valance band (VB) to the conduction band (CB) are allowed or prohibited, depending on the position of the Fermi level of graphene. For the unbiased ($V = 0$) VCG-gold-SA, the Fermi level (E_F) of graphene lies near the Dirac point and carrier transitions are allowed for an ultrabroad range of photon energies as shown in figure 1(b) (left sketch). For the biased case ($V \neq 0$), the Fermi level of the VCG-gold-SA shifts with respect to the Dirac point (right) and as is well known from Pauli exclusion principle, one-photon transitions of the carriers are prohibited for incident photons with energies less than $2E_F$. In this case, multi-photon absorption can occur at sufficiently high photon energies. During the transient absorption experiments, the Fermi level shift was obtained by applying a bias to the VCG-gold-SA and the resulting change in both types of nonlinear absorption (saturable and multi-photon) were investigated by using a femtosecond pump-probe setup.

The voltage-dependent ultrafast and nonlinear optical properties of the VCG-gold-SA were investigated by using a femtosecond transient absorption spectrometer (Helios, Ultrafast Systems) operating around visible and near-infrared wavelengths. In the experiments, the output of a tunable optical parametric amplifier (OPA) (Spectra-Physics, TOPAS Prime) which was pumped with a 1 kHz, 800 nm Ti^{3+} :sapphire regenerative amplifier (Spectra-Physics, Spitfire Ace, pulsewidth = 134 fs) was used to excite the VCG-gold-SA. The pump pulses at the wavelengths of 1000, 700, 650, and 470 nm were obtained by using sum-frequency, second-harmonic, and

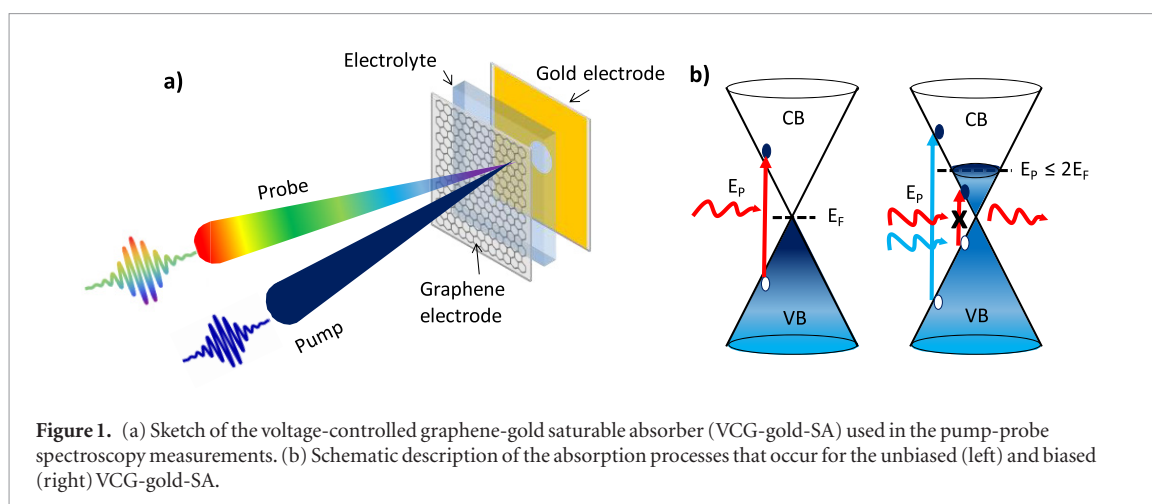


Figure 1. (a) Sketch of the voltage-controlled graphene-gold saturable absorber (VCG-gold-SA) used in the pump-probe spectroscopy measurements. (b) Schematic description of the absorption processes that occur for the unbiased (left) and biased (right) VCG-gold-SA.

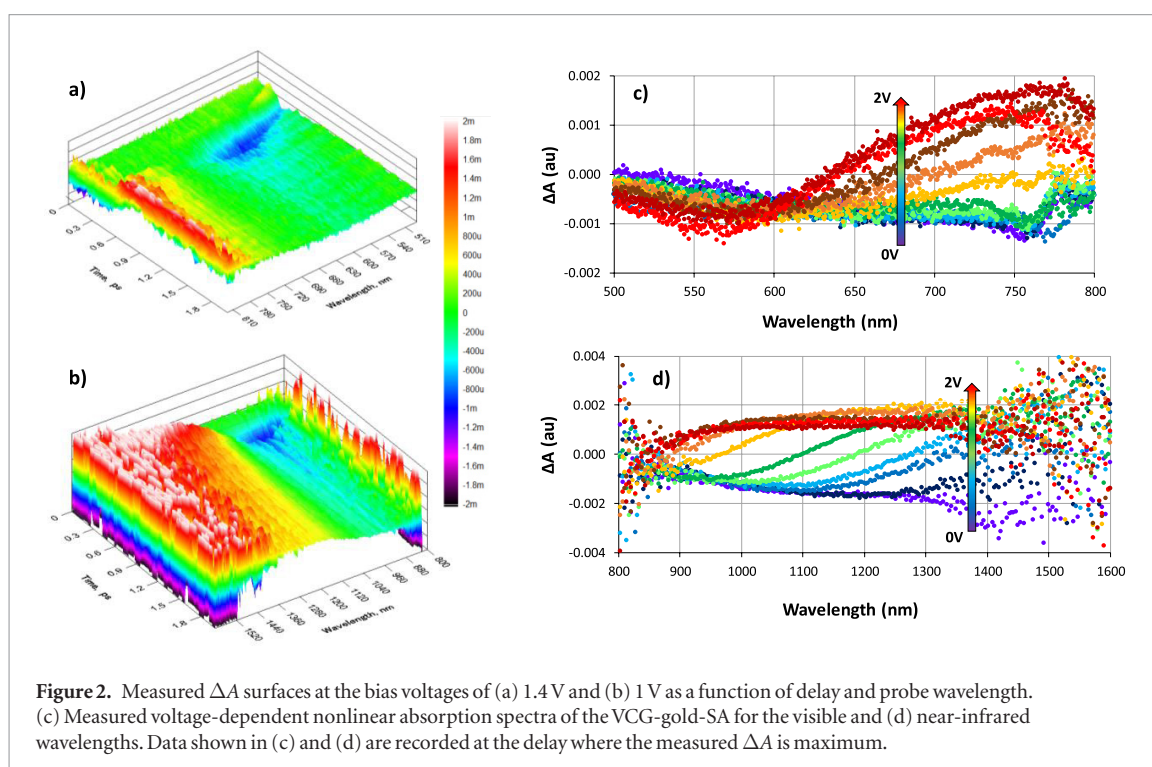


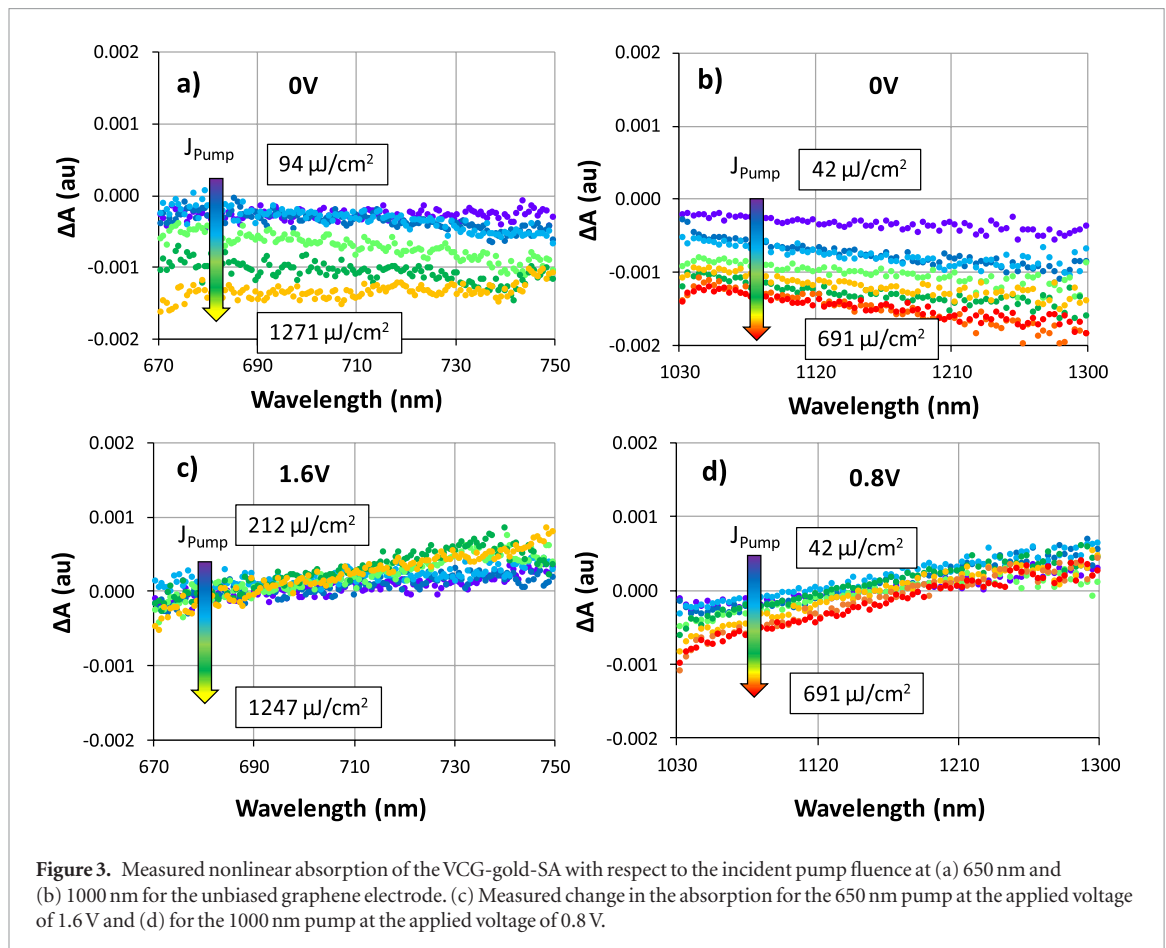
Figure 2. Measured ΔA surfaces at the bias voltages of (a) 1.4 V and (b) 1 V as a function of delay and probe wavelength. (c) Measured voltage-dependent nonlinear absorption spectra of the VCG-gold-SA for the visible and (d) near-infrared wavelengths. Data shown in (c) and (d) are recorded at the delay where the measured ΔA is maximum.

fourth-harmonic generation schemes of the OPA. The nonlinear absorption spectrum ΔA ($\Delta A =$ pumped absorption-unpumped absorption) of the VCG-gold-SA was then measured by using the visible (500–800 nm) and the near-infrared (800–1600 nm) white-light continuum probe pulses. A motorized optical delay line with a time resolution of 14 fs was used to introduce a time delay between the pump and probe pulses. Furthermore, the pump beam incident on the VCG-gold-SA was periodically blocked with a 500 Hz chopper to record the nonlinear ΔA spectrum. Note that the signal to noise ratio in the nonlinear absorption measurements decreased near the edges of the generated white-light continua as the intensity of the probe signal diminished (see figure 2). During the nonlinear absorption experiments, the pump spot size incident on the VCG-gold-SA was adjusted to be sufficiently larger than the probe spot size to ensure that all of the probed area was excited by the pump beam.

Furthermore, the incident probe fluence was kept at much lower levels than those of the pump to minimize probe-induced excitation of the VCG-gold-SA.

3. Results and discussion

To determine the spectral bandwidth of the voltage-dependent saturable absorption band of the VCG-gold-SA, 470 nm and 700 nm pump pulses were used and the nonlinear absorption spectra were measured by using the visible (500–800 nm) and near-infrared (800–1600 nm) white-light continuum probes. Figure 2 summarizes the measured voltage-dependent nonlinear absorption results for the VCG-gold-SA. In particular, figures 2(a) and (b) show the measured ΔA surface as a function of the probe wavelength and delay at the specific bias voltages of 1.4 V (figure 2(a)) and 1 V (figure 2(b)). Figures 2(c) and (d) further show the maximum measured ΔA (at the delay where



ΔA is maximum) as a function of probe wavelength at different bias voltages. Here, $\Delta A < 0$ corresponds to the case, where single-photon transitions of the excited carriers are allowed in the graphene electrode for photon energies $E_p > 2E_F$. If a bias is applied to vary the Fermi level position of the VCG-gold-SA, multiphoton absorption becomes dominant for photon energies $E_p < 2E_F$ ($\Delta A > 0$). As shown in figure 2, we have observed both regimes of absorption at the visible and near-infrared probe wavelengths by increasing the applied bias from 0 to 2 V.

For the experiments performed in the visible region (see figure 2(c)), the saturable absorption bandwidth of the VCG-gold-SA was measured to be around 120 nm (630–750 nm) at 1.2 V of applied bias. As the applied voltage was increased, the measured saturable absorption bandwidth decreased but remained around 40 nm (630–670 nm) at the applied bias of 1.6 V. This was wide enough to support femtosecond pulse generation. Note that although the behavior of the device is more complex as a function of bias and shows the opposite trends for wavelengths below 600 nm, the measured ΔA remains negative down to 500 nm indicating that the VCG-gold can still operate as a saturable absorber at these wavelengths.

Figure 2(d) shows the voltage-dependent nonlinear absorption measurements performed for the near-infrared wavelengths. At zero bias, the long wavelength limit of the saturable absorption band could not be determined due to the decrease in the signal to noise

ratio of the near-infrared continuum above 1400 nm. However, for bias voltages higher than 0.2 V, the long wavelength cut-off for the saturable absorption was readily determined. At 0.6 V of applied bias, the saturable absorber action of the VCG-gold-SA was completely blocked for wavelengths above 1300 nm.

Together with the nonlinear absorption measurements performed in the visible region, the spectral bandwidth for voltage-reconfigurable saturable absorption of the VCG-gold-SA was measured to be around 670 nm (630–1300 nm) at the applied bias of 0.6 V. As expected, the measured bandwidth decreased to 470 nm (630–1100 nm) at 1 V of applied bias, but remained sufficiently wide to enable femtosecond pulse generation from lasers operating around near-infrared wavelengths. Note that for the wavelengths higher than about 1050 nm, we observed a decrease in the measured multi-photon absorption for applied voltages beyond 1.6 V. This behavior was somewhat similar to the opposite trend which was observed for wavelengths below 600 nm and requires further investigation.

The results shown in figure 2 clearly demonstrate that the VCG-gold-SA with bias-controlled absorption could be used as a mode locking element over a broad wavelength range. Hence, it is also important to determine the voltage-dependent saturable absorber characteristics (such as saturation fluence and modulation depth) of the VCG-gold-SA. For this purpose, the fluence of the 650 nm (1000 nm) pump incident

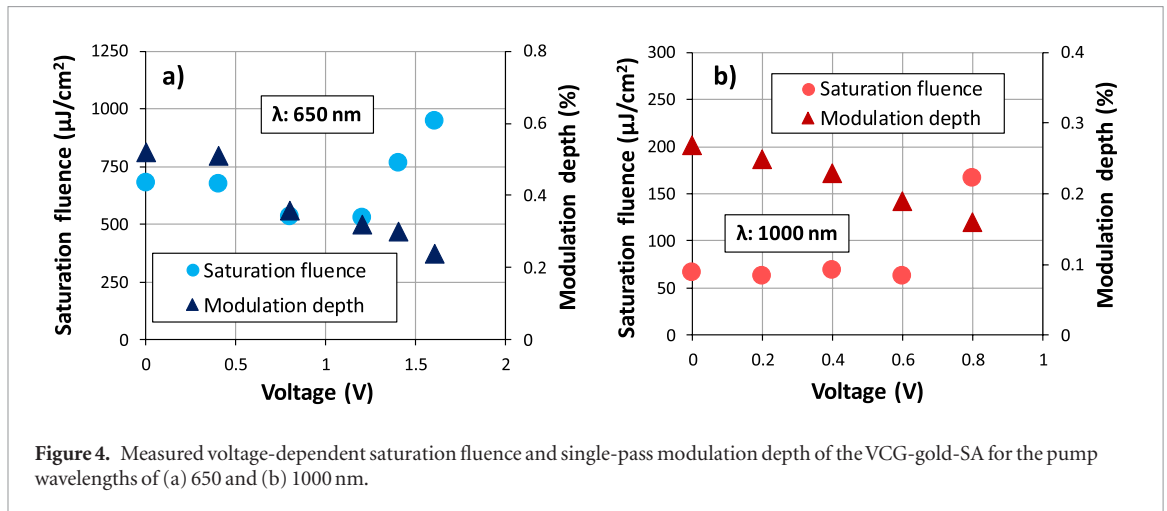


Figure 4. Measured voltage-dependent saturation fluence and single-pass modulation depth of the VCG-gold-SA for the pump wavelengths of (a) 650 and (b) 1000 nm.

on the VCG-gold-SA was varied and the change in the nonlinear ΔA spectrum was measured with respect to the applied voltage. Figure 3 summarizes the intensity-dependent nonlinear absorption results obtained for the selected voltages of 0, 0.8, and 1.6 V. In the experiments, the nonlinear absorption response of the VCG-gold-SA was probed at wavelengths higher than the selected pump wavelengths of 650 and 1000 nm. As can be seen from figures 3(a) and (b), the VCG-gold-SA retained its saturable absorption bandwidth over a broad wavelength range of 670–750 nm and 1030–1300 nm. For the applied voltages beyond 1.6 V (0.8 V), the multi-photon absorption was already effective at the wavelengths higher than around 690 nm (1200 nm), as expected from the nonlinear absorption measurements (see figures 3(c) and (d)).

By using

$$\Delta A = -\frac{q_0}{T \ln 10} \left[1 - \frac{J_{\text{sat}}}{J_p} \left(1 - e^{-\frac{J_p}{J_{\text{sat}}}} \right) \right], \quad (1)$$

the voltage-dependent saturation fluence (J_{sat}) and the single-pass modulation depth (q_0) of the VCG-gold-SA were estimated for the pump wavelengths of 650 and 1000 nm [54]. In equation (1), T is the voltage-dependent steady-state transmission of the VCG-gold-SA at the pump wavelength and J_p is the incident pump fluence. Figures 4(a) and (b) summarize the results obtained for the $\Delta A < 0$ regime. Similar to previous studies [52, 53], we obtained lower saturation fluences and smaller modulation depths for the near-infrared pump compared to the visible pump. For the unbiased case (0 V), the estimated saturation fluence and single-pass modulation depth of the VCG-gold-SA were 682 $\mu\text{J cm}^{-2}$ (67.5 $\mu\text{J cm}^{-2}$) and 0.52% (0.27%) at the pump wavelength of 650 nm (1000 nm). As can be seen from figure 4, the single-pass modulation depth of the graphene electrode monotonically decreased from 0.52% (0.27%) to 0.24% (0.16%) at the pump wavelength of 650 nm (1000 nm). Furthermore, as the applied bias was increased from 0 to 1.6 V (0.8 V), the estimated saturation fluence increased up to 951 $\mu\text{J cm}^{-2}$ (168 $\mu\text{J cm}^{-2}$) at the pump wavelength of 650 nm (1000 nm).

Table 1. Measured voltage-dependent saturation fluence and single-pass modulation depth for the pump wavelengths of 650 and 1000 nm for the multi-photon absorption regime.

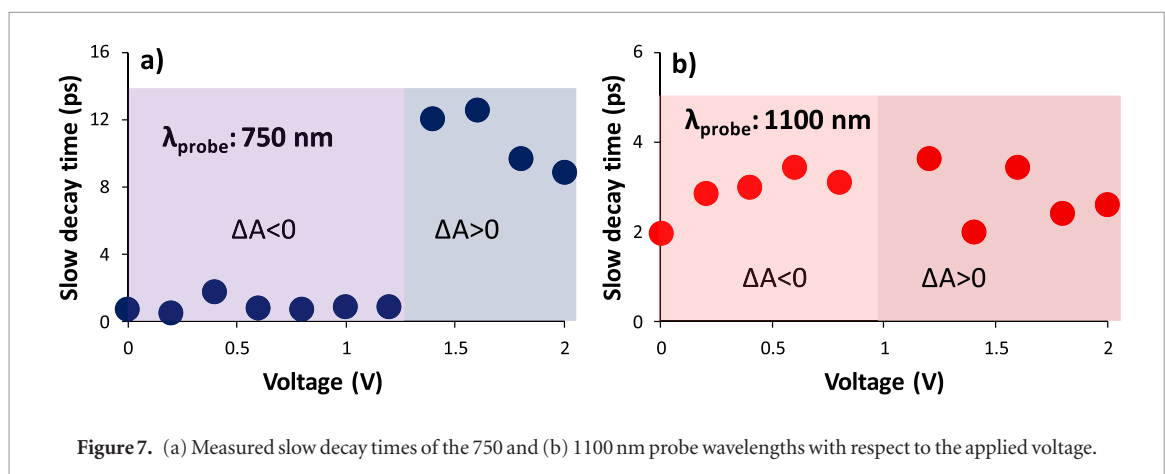
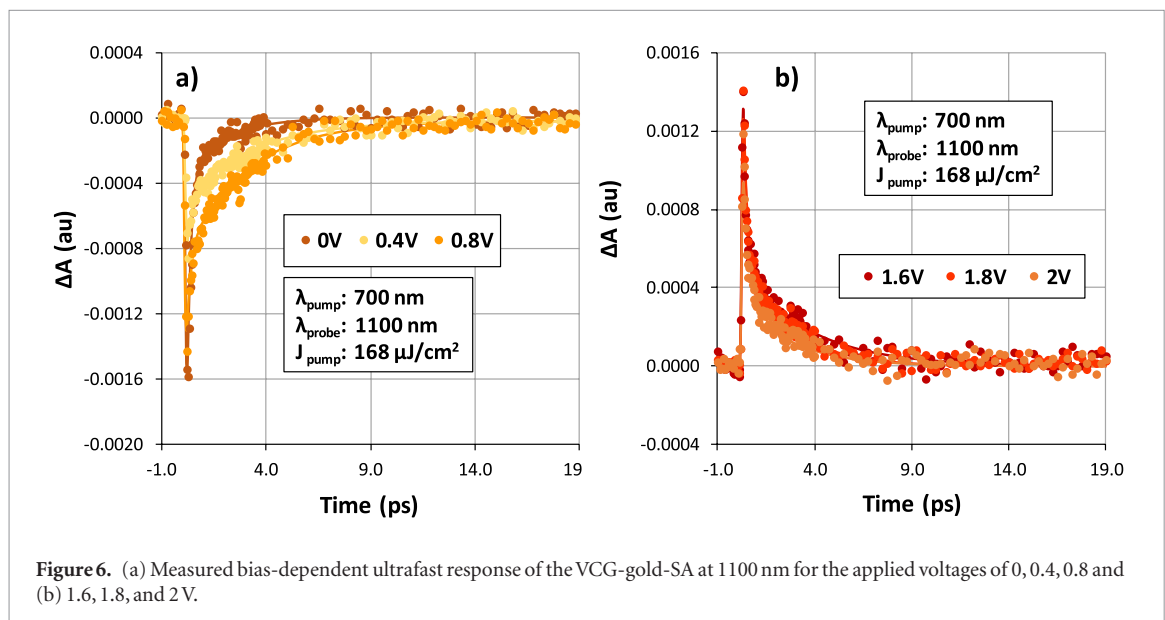
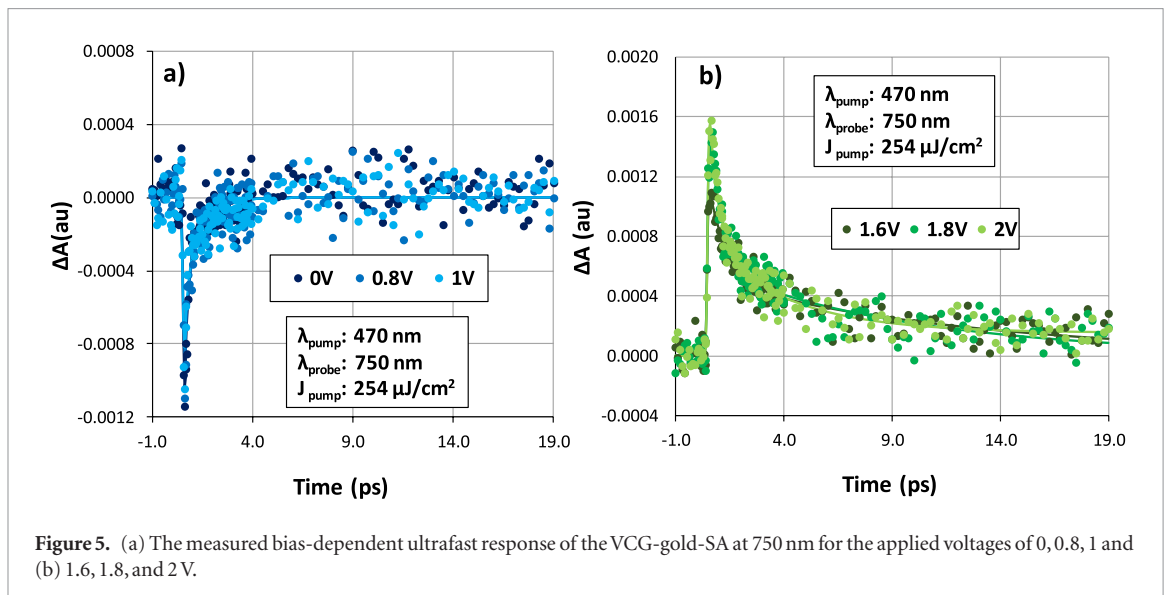
Voltage (V)	1000 nm		650 nm	
	Mod. depth (%)	Sat. fluence ($\mu\text{J cm}^{-2}$)	Mod. depth (%)	Sat. fluence ($\mu\text{J cm}^{-2}$)
1	0.1	62	—	—
1.2	0.2	80	—	—
1.4	0.26	243	—	—
1.6	0.18	265	—	—
1.8	0.14	219	0.21	689
2	0.19	456	0.17	407

We have also estimated the voltage-dependent saturation fluence and modulation depth of the VCG-gold-SA for the multi-photon absorption regimes ($\Delta A > 0$) of both pump wavelengths. The results are summarized in table 1.

The decay time of a saturable absorber is also an important parameter which determines the ultra-short pulse generation ability of a mode locking element. Hence, the bias-dependent decay times of the VCG-gold-SA were further investigated by using the same femtosecond pump-probe spectrometer. Figures 5–7 summarize the results obtained for the visible (750 nm) and near-infrared (1100 nm) probe wavelengths. As expected from the nonlinear absorption measurements, decay dynamics with $\Delta A < 0$ and $\Delta A > 0$ were obtained depending on the applied voltage.

For the 750 nm probe, the measured slow decay times were comparable to previously reported values [13] for the $\Delta A < 0$ regime (see figure 5(a)). When one-photon transitions were blocked ($\Delta A > 0$), the measured slow decay times increased from 0.9 (0–1.2 V) to around 10.7 ps (1.4–2 V) as a result of the longer relaxation pathway for the predominant multi-photon absorption (see figures 5(b) and 7(a)) of the 750 nm probe.

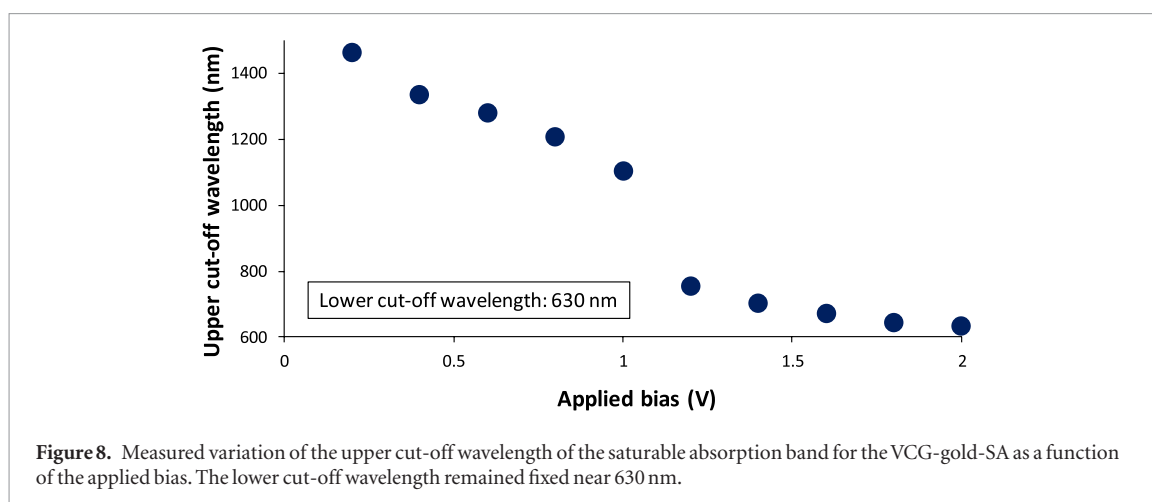
For the pump-probe measurements performed in the near-infrared wavelengths, the measured slow decay times remained around 2.8 ± 0.5 ps as the



applied bias was increased from 0 to 2 V (see figures 6 and 7(b)). Although the measured slow time constants of the graphene electrode showed a tendency to increase with increasing bias for both $\Delta A < 0$ and $\Delta A > 0$ regions, there was no evident correlation between the decay time of the slow relaxation

process and the applied voltage, especially in the $\Delta A > 0$ region of the near-infrared wavelengths (see figure 7(b)).

During the pump-probe experiments, the duration of the probe pulse (>134 fs) was not short enough to resolve the fast decay time of the graphene electrode.



Hence, the fast time constants of both cases (visible and near-infrared) could not be measured accurately.

4. Conclusions

In conclusion, we have described a detailed set of pump-probe experiments to investigate the fast saturable absorber characteristics of VCG-gold-SA as a function of bias voltage. The most important result of the study is that at bias voltages needed to adjust the linear absorption (and hence, the insertion loss), the VCG-gold-SA maintains its saturable absorber property over a sufficiently wide spectral range to enable femtosecond pulse generation. For example, at the bias voltage of 1 V, the saturable absorption band has a width of 470 nm, extending from 630 nm to 1100 nm. Measurements indicate that the lower cut-off wavelength of the saturable absorption band remains approximately fixed near 630 nm as the bias voltage is increased. However, the upper cut-off wavelength of the saturable absorption band decreases with increasing bias as displayed in figure 8 due to Pauli blocking. Figure 8 shows the cut-off wavelengths which were determined from this study. Since the voltage-controlled saturable absorption could be obtained for the wavelengths as low as 630 nm, figure 8 clearly demonstrates that it is possible to obtain a 470 nm (630–1100 nm) wide saturable absorption bandwidth for the VCG-gold-SA at 1 V of applied bias. Alternatively, if we interpret the cut-off wavelength as the operating wavelength of the device, the corresponding voltage refers to the maximum voltage where VCG-gold-SA functions effectively as a mode locker with adjustable insertion loss. In our previous studies, we tested the mode locking performance of the VCG-gold-SA at the wavelengths of 800 and 1250 nm. The bias range in which the device could be used for femtosecond pulse generation was in fair agreement with the data displayed in figure 8 [48–50].

During the experiments, the saturable absorber parameters such as the saturation fluence, modulation depth, and decay time of the VCG-gold-SA were further measured as a function of the applied voltage.

Our experimental results were in agreement with the theoretical predictions that were reported by previous studies [52, 53]. The results obtained for the 650 nm (1000 nm) pump demonstrated that the single-pass modulation depth of the VCG-gold-SA decreased from 0.52% (0.27%) to 0.24% (0.16%) and the saturation fluence increased from $682 \mu\text{J cm}^{-2}$ ($67.5 \mu\text{J cm}^{-2}$) to $951 \mu\text{J cm}^{-2}$ ($168 \mu\text{J cm}^{-2}$) as the applied bias was varied between 0 and 1.6 V (0.8 V). The bias-dependent saturation fluence values fall within a range which can be obtained in practice by adjusting the spot size on the VCG-gold-SA or by increasing the intracavity energy of the laser. Finally, the voltage-dependent slow decay times of the VCG-gold-SA remained in the range of 1–3 ps for the saturable absorption regime (750 nm probe), as expected. For the multi-photon absorption regime, the increased pathway for the relaxation process led to an increase in the measured slow decay times (10.7 ps) with the 750 nm probe.

The experimental results of this study clearly suggest that under bias voltages in the range of 0–2 V, it should be possible to adjust the insertion loss of the VCG-gold-SA and at the same time, maintain a sufficient amount of modulation depth and an attainable level of saturation fluence over an ultrabroad spectral bandwidth for femtosecond pulse generation from lasers operating in the visible and near-infrared wavelengths.

ORCID iDs

I Baylam <https://orcid.org/0000-0003-2327-9035>

N Kakenov <https://orcid.org/0000-0003-2321-6157>

References

- [1] Novoselov K S, Falco V I, Colombo L, Gellert P R, Schwab M G and Kim K 2012 A roadmap for graphene *Nature* **490** 192–200
- [2] Anton A, Henri J, Yunyun D, Yadong W, Harri L and Zhippei S 2018 Nonlinear optics with 2D layered materials *Adv. Mater.* **30** 1705963
- [3] Ferrari A C *et al* 2006 Raman spectrum of graphene and graphene layers *Phys. Rev. Lett.* **97** 187401

- [4] Kuzmenko A B, van Heumen E, Carbone F and van der Marel D 2008 Universal optical conductance of graphite *Phys. Rev. Lett.* **100** 117401
- [5] Zhang H, Virally S, Bao Q, Ping L K, Massar S, Godbout N and Kockaert P 2012 Z-scan measurement of the nonlinear refractive index of graphene *Opt. Lett.* **37** 1856–8
- [6] Bonaccorso F, Sun Z, Hasan T and Ferrari A C 2010 Graphene photonics and optoelectronics *Nat. Photon.* **4** 611–22
- [7] Falkovsky L A 2008 Optical properties of graphene *J. Phys.: Conf. Ser.* **129** 012004
- [8] Bao Q, Zhang H, Wang Y, Ni Z, Yan Y, Shen Z X, Loh K P and Tang D Y 2009 Atomic-layer graphene as a saturable absorber for ultrafast pulsed lasers *Adv. Funct. Mater.* **19** 3077–83
- [9] Mak K F, Ju L, Wang F and Heinz T F 2012 Optical spectroscopy of graphene: from the far infrared to the ultraviolet *Solid State Commun.* **152** 1341–9
- [10] Ahn K J, Gwak J Y, Lee B J, Choi S Y, Kim M H, Baek I H, Jeong Y U and Rotermund F 2017 Wavelength and fluence-dependent third-order optical nonlinearity of mono- and multi-layer graphene *Appl. Opt.* **56** 9920–4
- [11] Ferrante C et al 2018 Raman spectroscopy of graphene under ultrafast laser excitation *Nat. Commun.* **9** 308
- [12] Dhanabalan S C, Ponraj J S, Zhang H and Bao Q 2016 Present perspectives of broadband photodetectors based on nanobelts, nanoribbons, nanosheets and the emerging 2D materials *Nanoscale* **8** 6410–34
- [13] Dawlaty J M, Shivaraman S, Chandrashekar M, Rana F and Spencer M G 2008 Measurement of ultrafast carrier dynamics in epitaxial graphene *Appl. Phys. Lett.* **92** 042116
- [14] George P A, Strait J, Dawlaty J, Shivaraman S, Chandrashekar M, Rana F and Spencer M G 2008 Ultrafast optical-pump terahertz-probe spectroscopy of the carrier relaxation and recombination dynamics in epitaxial graphene *Nano Lett.* **8** 4248–51
- [15] Sun D, Wu Z K, Divin C, Li X, Berger C, de Heer W A, First P N and Norris T B 2008 Ultrafast relaxation of excited Dirac fermions in epitaxial graphene using optical differential transmission spectroscopy *Phys. Rev. Lett.* **101** 157402
- [16] Dani K M, Lee J, Sharma R, Mohite A D, Galande C M, Ajayan P M, Dattelbaum A M, Htoon H, Taylor A J and Prasankumar R P 2012 Intraband conductivity response in graphene observed using ultrafast infrared-pump visible-probe spectroscopy *Phys. Rev. B* **86** 125403
- [17] Winnerl S 2013 Time-resolved spectroscopy on epitaxial graphene in the infrared spectral range: relaxation dynamics and saturation behavior *J. Phys.: Condens. Matter* **25** 054202
- [18] Brida D et al 2013 Ultrafast collinear scattering and carrier multiplication in graphene *Nat. Commun.* **4** 1987
- [19] Malard L M, Mak K F, Neto A H C, Peres N M R and Heinz T F 2013 Observation of intra- and inter-band transitions in the transient optical response of graphene *New J. Phys.* **15** 015009
- [20] Oum K, Lenzer T, Scholz M, Jung D Y, Sul O, Cho B J, Lange J and Müller A 2014 Observation of ultrafast carrier dynamics and phonon relaxation of graphene from the deep-ultraviolet to the visible region *J. Phys. Chem. C* **118** 6454–61
- [21] Kurum U, Ekiz O O, Yaglioglu H G, Elmali A and Urel M 2011 Electrochemically tunable ultrafast optical response of graphene oxide *Appl. Phys. Lett.* **98** 141103
- [22] Kadi F, Winzer T, Knorr A and Malic E 2015 Impact of doping on the carrier dynamics in graphene *Sci. Rep.* **5** 16841
- [23] Tomadin A et al 2018 The ultrafast dynamics and conductivity of photoexcited graphene at different Fermi energies *Sci. Adv.* **4** 5313
- [24] Lee C C, Mohr C, Bethge J, Suzuki S, Fermann M E, Hartl I and Schibli T R 2012 Frequency comb stabilization with bandwidth beyond the limit of gain lifetime by an intracavity graphene electro-optic modulator *Opt. Lett.* **37** 3084–6
- [25] Balci O, Kakenov N, Karademir E, Balci S, Cakmakyan S, Polat E O, Caglayan H, Ozbay E and Kocabas C 2018 Electrically switchable metadevices via graphene *Sci. Adv.* **4** 1749
- [26] Zhang A, Lu W, Liu Z, Chen H and Huang B 2018 Dynamically tunable substrate-integrated-waveguide attenuator using graphene *IEEE Trans. Microw. Theory Tech.* **66** 3081–9
- [27] Kakenov N, Balci O, Takan T, Ozkan V A, Altan H and Kocabas C 2016 Observation of gate-tunable coherent perfect absorption of terahertz radiation in graphene *ACS Photon.* **3** 1531–5
- [28] Yao Y, Shankar R, Kats M A, Song Y, Kong J, Loncar M and Capasso F 2014 Electrically tunable metasurface perfect absorbers for ultrathin mid-infrared optical modulators *Nano Lett.* **14** 6526–32
- [29] Thareja V, Kang J H, Yuan H, Milaninia K M, Hwang H Y, Cui Y, Kik P G and Brongersma M L 2015 Electrically tunable coherent optical absorption in graphene with ion gel *Nano Lett.* **15** 1570–6
- [30] Hwang M-S et al 2017 Switching of photonic crystal lasers by graphene *Nano Lett.* **17** 1892–8
- [31] Polat E O and Kocabas C 2013 Broadband optical modulators based on graphene supercapacitors *Nano Lett.* **13** 5851–7
- [32] Liu M, Yin X B, Ulin-Avila E, Geng B S, Zentgraf T, Ju L, Wang F and Zhang X 2011 A graphene-based broadband optical modulator *Nature* **474** 64–7
- [33] Kim S, Jang M S, Brar V W, Mauer K W, Kim L and Atwater H A 2018 Electronically tunable perfect absorption in graphene *Nano Lett.* **18** 971–9
- [34] Balci O, Polat E O, Kakenov N and Kocabas C 2015 Graphene-enabled electrically switchable radar-absorbing surfaces *Nat. Commun.* **6** 6628
- [35] Polat E O, Balci O, Kakenov N, Uzlu H B, Kocabas C and Dahiya R 2015 Synthesis of large area graphene for high performance in flexible optoelectronic devices *Sci. Rep.* **5** 16744
- [36] Yao B et al 2018 Gate-tunable frequency combs in graphene-nitride microresonators *Nature* **558** 410–4
- [37] Soavi G et al 2018 Broadband, electrically tunable third-harmonic generation in graphene *Nat. Nanotechnol.* **13** 583–8
- [38] Jiang T et al 2018 Gate-tunable third-order nonlinear optical response of massless Dirac fermions in graphene *Nat. Photon.* **12** 430–6
- [39] Cihan C, Kocabas C, Demirbas U and Sennaroglu A 2018 Graphene mode-locked femtosecond Alexandrite laser *Opt. Lett.* **43** 3969–72
- [40] Baek I H, Lee H W, Bae S, Hong B H, Ahn Y H, Yeom D-I and Rotermund F 2012 Efficient mode-locking of sub-70-fs Ti:sapphire laser by graphene saturable absorber *Appl. Phys. Express* **5** 032701
- [41] Ozharar S, Baylam I, Cizmeciyan M N, Balci O, Pince E, Kocabas C and Sennaroglu A 2013 Graphene mode-locked multipass-cavity femtosecond Cr⁴⁺:forsterite laser *J. Opt. Soc. Am. B* **30** 1270–5
- [42] Tolstik N, Sorokin E and Sorokina I T 2014 Graphene mode-locked Cr:ZnS laser with 41 fs pulse duration *Opt. Express* **22** 5564–71
- [43] Cizmeciyan M N, Kim J W, Bae S, Hong B H, Rotermund F and Sennaroglu A 2013 Graphene mode-locked femtosecond Cr:ZnSe laser at 2500 nm *Opt. Lett.* **38** 341–3
- [44] Canbaz F, Kakenov N, Kocabas C, Demirbas U and Sennaroglu A 2017 Generation of sub-20 fs pulses from a graphene mode-locked laser *Opt. Express* **25** 2834–9
- [45] Davide Di Dio Cafiso S et al 2013 Sub-100 fs Cr:YAG laser mode-locked by monolayer graphene saturable absorber *Opt. Lett.* **38** 1745–7
- [46] Zhu G, Zhu X, Wang F, Xu S, Li Y, Guo X, Balakrishnan K, Norwood R A and Peyghambarian N 2016 Graphene mode-locked fiber laser at 2.8 μm *IEEE Photon. Technol. Lett.* **28** 7–10
- [47] Lagatsky A A et al 2013 2 μm solid-state laser mode-locked by single-layer graphene *Appl. Phys. Lett.* **102** 013113
- [48] Baylam I, Ozharar S, Kakenov N, Kocabas C and Sennaroglu A 2017 Femtosecond pulse generation from a Ti³⁺:sapphire laser near 800 nm with voltage reconfigurable graphene saturable absorbers *Opt. Lett.* **42** 1404–7
- [49] Baylam I, Balci O, Kakenov N, Kocabas C and Sennaroglu A 2016 Graphene-gold supercapacitor as a voltage controlled saturable absorber for femtosecond pulse generation *Opt. Lett.* **41** 910–3
- [50] Baylam I, Cizmeciyan M N, Ozharar S, Polat E O, Kocabas C and Sennaroglu A 2014 Femtosecond pulse generation with

- voltage-controlled graphene saturable absorber *Opt. Lett.* [39](#) 5180–3
- [51] Lee E J *et al* 2015 Active control of all-fibre graphene devices with electrical gating *Nat. Commun.* [6](#) 6851
- [52] Marini A, Cox J D and Garcia de Abajo F J 2017 Theory of graphene saturable absorption *Phys. Rev. B* [95](#) 125408
- [53] Vasko F T 2010 Saturation of interband absorption in graphene *Phys. Rev. B* [82](#) 245422
- [54] Sennaroglu A, Demirbas U, Ozharar S and Yaman F 2006 Accurate determination of saturation parameters for Cr⁴⁺-doped solid-state saturable absorbers *J. Opt. Soc. Am. B* [23](#) 241–9